J Solid State Electrochem (2004) 8: 644–649
DOI 10.1007/s10008-004-0505-1

ORIGINAL PAPER

D. Pérez-Coll · P. Núñez · D. Marrero-López
J. C. C. Abrantes · J. R. Frade

Effects of sintering additives on the mixed transport properties of ceria-based materials under reducing conditions

Received: 11 April 2003 / Accepted: 29 September 2003 / Published online: 5 March 2004

Abstract Commercial $Ce_{0.8}Gd_{0.2}O_{2-\delta}$ nanopowders and alternative precursors synthesized by a freeze-drying method were used to obtain samples with and without Co addition as a sintering agent. Two percent Co-doped samples were sintered at 1150 °C and 1500 °C and undoped samples were sintered at 1500 °C or 1600 °C to obtain samples with relative densities in the range 92–94%. The total conductivity and the relative roles of bulk and grain boundary conductivity were studied by impedance spectroscopy. These results demonstrated that additions of Co play a very significant effect on the grain boundary behaviour, which is spoiled when the sintering temperature is excessive. Significant differences in grain boundary behaviour were also found between samples prepared from different precursor powders. The electronic conductivity of these materials was evaluated by an ion-blocking method and revealed that samples containing Co additions as a sintering additive possess somewhat lower n-type conductivity under identical conditions of temperature and oxygen partial pressure. The differences tend to vanish when these Co-doped samples are fired at high temperatures (1500 °C).

Keywords Cobalt-doped ceria · Electronic conductivity · Ion blocking · n-type conductivity · Sintering additives

Presented at the OSSEP Workshop "Ionic and Mixed Conductors: Methods and Processes", Aveiro, Portugal, 10–12 April 2003

D. Pérez-Coll · P. Núñez (✉) · D. Marrero-López
Departamento de Química Inorgánica, Universidad de La Laguna, 38200 La Laguna, Tenerife, Spain
E-mail: pnunez@ull.es
Tel.: +34-922-318501
Fax: +34-922-318461

J. C. C. Abrantes
ESTG, Instituto Politécnico de Viana do Castelo, 4900 Viana do Castelo, Portugal

J. R. Frade
Departamento de Engenharia Cerâmica e do Vidro, CICECO, Universidade de Aveiro, 3810-193 Aveiro, Portugal

Abbreviations

CGO	$Ce_{0.8}Gd_{0.2}O_{1.9}$
FD	freeze-dried
RH	rhodia

Introduction

Ceria-based materials have attracted great interest as potential solid electrolytes for application in electrochemical devices operating in the temperature range 500–700 °C, because they possess higher ionic conductivity than the standard yttria-stabilized zirconia [1, 2, 3, 4]. One of the main limitations of these solid electrolytes is their mechanical weakness, especially for samples with relatively large grain sizes. However, it was recently reported [4] that the addition of small amounts of cobalt oxide to ceria-based nanopowders allows densification at temperatures as low as 900 °C, with grain sizes smaller than 100 nm. These results were confirmed by others [5], achieving about 95% dense pellets after firing at 900 °C for 2 hours, with grain sizes in the range of 100–200 nm.

It was reported [4] that sintering of $Ce_{0.8}Gd_{0.2}O_{1.9}$ (CGO) was facilitated by a residual grain boundary amorphous phase, with a typical thickness of several nanometres. Other authors [6] expressed a different interpretation for the enhanced sinterability by analysing differential thermal analysis (DTA) results of the decomposition of $Co(NO_3)_2.6H_2O$ dissolved in ethanol and subsequently dried in air in order to investigate the role of Co_3O_4 in the sintering mechanism. They reported an endothermic peak at about 900 °C, ascribed to the conversion of Co_3O_4 to CoO, and suggested that this reaction was responsible for the improved densification. Others [7] reported a combined thermal gravimetric and differential thermal analysis (TG + DTA) and observed exothermic peaks at 850 °C and at 950 °C. They attributed the exothermal peak at 850 °C to the transition of Co_2O_3 into Co_3O_4 and the peak at 950 °C to the transition of Co_3O_4 to CoO. Kleinlogel and Gauckler [4] reported that addition of Co to CGO in the form of

$Co(NO_3)_2.6H_2O$ leads to a thin film of Co_3O_4 after decomposition of the nitrates at 350 °C, and ascribed the enhanced densification of CGO to melting of the cobalt oxide film at 900 °C. It was also reported that cobalt oxide dissolves in CGO at higher sintering temperatures, resulting in the disappearance of the liquid thin film [5].

Less attention has been dedicated to the effects of Co additions on the transport properties. Results on the total conductivity of 2% Co-doped CGO as a function of oxygen partial pressure indicated that doping does not significantly alter the oxygen ionic conductivity and the electrolytic domain compared to pure CGO [4, 6]. However, these conclusions were based on the dependence of conductivity on oxygen partial pressure, which provides limited and rather indirect information on the electronic conductivity. For example, the dependence of total conductivity on oxygen partial pressure may be insufficient to separate the ionic and electronic contributions when both vary simultaneously. This may be the case for ceria-based materials with relatively high oxygen deficiency [8]. One must thus resort to techniques which give a direct measurement of the electronic conductivity (e.g. the Hebb–Wagner ion-blocking method [9, 10, 11]), or direct measurements of the ionic transport number (e.g. e.m.f. measurements or faradaic efficiency measurements).

In addition, one should re-examine the effects of the additives on grain boundary behaviour, especially for samples with sub-micrometric grain size, as found for Co-doped samples sintered at 900–1000 °C. Note that the grain boundary resistance of ceria-based materials with average grain size above 1 μm is far from negligible at temperatures lower than about 500 °C [12, 13, 14] and a simple brick-layer model predicts an increase in grain boundary resistance by one order of magnitude on lowering the average grain size from 1 μm to 0.1 μm. Exceptions might thus suggest major changes in grain boundary behaviour, caused by selective segregation at grain boundaries, deliberate composition changes, etc. This might explain the grain boundary behaviour of CGO materials with a Co-rich grain boundary shell, fired at relatively low temperatures [4].

Experimental

Powder preparation and sintering of pellets

Commercial $Ce_{0.8}Gd_{0.2}O_{2-\delta}$ (CGO) powder (Rhodia, Frankfurt, Germany), with a crystallite size of 20 nm and a specific surface area of about 26 $m^2\ g^{-1}$, was used as one of the starting materials (RH). For comparison, a freeze-dried method was used to prepare an alternative CGO precursor powder (FD), using a method described elsewhere [15]. The starting powders were mixed with cobalt nitrate [$Co(NO_3)_2.6H_2O$, Merck] dissolved in ethanol, in a proportion corresponding to 2 mol% Co. The Co-doped powders were dried and then calcined at 650 °C for 1 h. Cylindrical pellets of 10 and 20 mm in diameter and a thickness of about 2 mm were obtained by uniaxial pressing at 3 tonnes for 30 s. Cobalt-doped pellets were sintered at 1150 °C and 1500 °C for 10 h using heating/cooling rates of 5 °C/min. Pellets of undoped $Ce_{0.8}Gd_{0.2}O_{2-\delta}$ were also sintered at 1500 °C, for a sample prepared from the Rhodia powder, and 1600 °C, for a sample from the freeze-dried precursor. The final density of each sintered sample (Table 1) was determined by the Archimedes method. XRD patterns showed no evidence of secondary phases. Sintered pellets were polished and thermally etched at a temperature 10% below the sintering temperature, for 30 min, to obtain scanning electron micrographs.

Electrical characterization

Pt electrodes with 5.5 mm diameter were painted on both surfaces of disks and fired at 1000 °C for 30 min. The total conductivity was evaluated by impedance spectroscopy, using a frequency response analyser (Solartron 1260). Impedance spectra were obtained in the frequency range 1–10^6 Hz, with an excitation voltage of 15 mV for the range 500–1000 °C and 250 mV for the range 200–500 °C. The low-temperature range (200–500 °C) allowed a separation of contributions ascribed to the bulk, internal interfaces and external material/electrode interfaces.

Ion-blocking Hebb–Wagner measurements were performed to measure the n-type conductivity. Cylindrical impervious pellets were used for this purpose, with painted Pt electrodes on both surfaces and an impervious alumina disk sealed on one side of the sample, thus providing an ion-blocking electrode under cathodic polarization. Ion-blocking measurements were performed for temperatures in the range 800–1000 °C under an increasing applied d.c. voltage (V_B), with 25 mV steps up to 1200 mV, using a Yokogawa 7651 d.c. source. An auxiliary known resistance, R_{aux}, was employed and the voltage drop in this resistance was used to obtain the current across the cell, $I = V_R/R_{aux}$. A different pair of Pt wires was used to measure the voltage in the cell (V_0), using a Keithley 2700 multimeter/data acquisition system.

Results and discussion

Microstructural effects on conductivity

Table 1 summarizes the values of the sintering temperature and relative density of the samples. Pellets with 2% Co and sintered at 1150 °C densify to 92–94% of the theoretical density, whereas undoped samples require 1500 °C to reach similar density values. Figure 1a and Fig. 1b show SEM images of the sintered pellets RH1500 and FD1600, prepared as indicated in Table 1.

Table 1 Relative density of ceria-based materials, prepared from commercial powders (RH) or from a freeze-dried precursor (FD), versus sintering temperature and time

Notation	Precursor	Co	T (°C)	t (h)	Relative density (%)
RHCo1150	Rhodia	2%	1150	10	94
RHCo1500	Rhodia	2%	1500	10	92
RH1500	Rhodia	–	1500	10	94
FDCo1150	Freeze-dried	2%	1150	10	92
FDCo1500	Freeze-dried	2%	1500	10	92
FD1600	Freeze-dried	–	1600	10	96

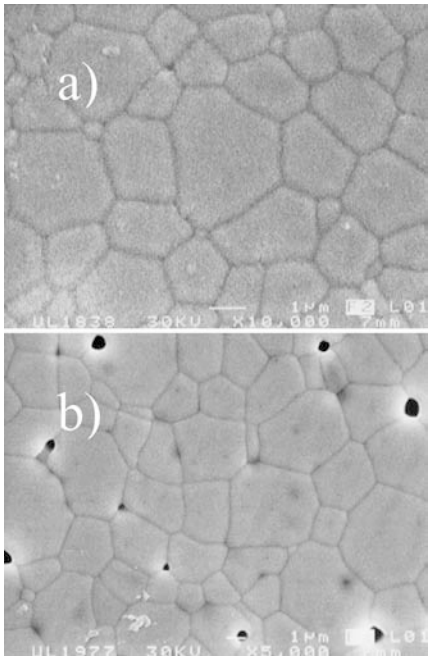

Fig. 1 Scanning electron micrographs of the samples a) RH1500 and b) FD1600

The commercial precursor yields slightly smaller average grain sizes, due to the difference in sintering temperature. Samples sintered at 1150 °C with Co addition possess much smaller grain sizes.

Differences in preparation, and the corresponding microstructural differences, often play significant effects on grain boundary conductivity. Impedance spectroscopy was thus used to analyse the relative contributions of the bulk and grain boundaries, based on the corresponding differences in relaxation frequencies and capacitance values. Typical examples are shown in Fig. 2 for samples FDCo1150. Since the bulk and grain boundary arcs are somewhat depressed, fitting was performed assuming a series association of (RQ) terms, and these fitting parameters were used to obtain the bulk conductivity (Fig. 3) and the grain boundary resistance results shown in Fig. 4, using typical Arrhenius representations:

$$\ln(\sigma T) = \ln(\sigma_0) - \frac{E_a}{kT} \quad (1)$$

A summary of the relevant parameters is shown in Table 2.

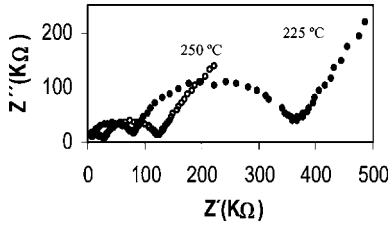

Fig. 2 Impedance spectra of sample FDCo1150

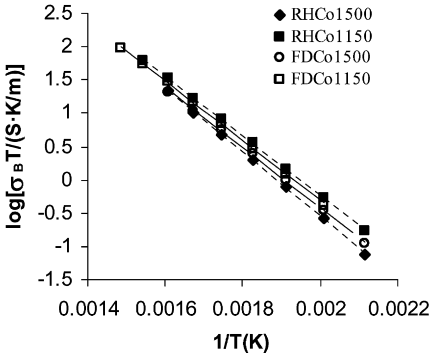

Fig. 3 Bulk conductivity results for the samples RHCo1150, RHCo1500, FDCo1150 and FDCo1500

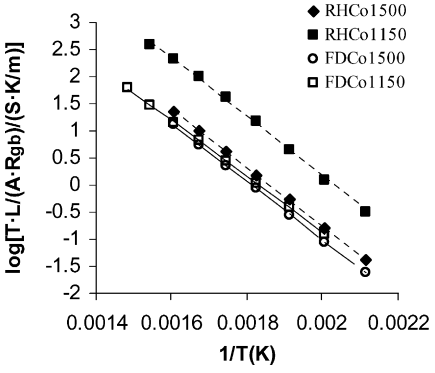

Fig. 4 Grain boundary results for the samples RHCo1150, RHCo1500, FDCo1150 and FDCo1500

The relaxation frequencies increase with temperature and thus the grain boundary and the bulk process could not be separated above 400 °C. Above this temperature, one can only extract the value of the total conductivity, $\sigma = L/(AR)$. The temperature dependence of the total conductivity in this high-temperature range (Fig. 5) yields smaller estimates of the activation energy. The apparent increase in activation energy with decreasing temperature can be explained by considering the increasing role of the grain boundary contribution, and possibly also interactions between oxygen vacancies and trivalent cations (Gd^{3+}) [16].

The results presented in Table 2 show that the conductivity of samples sintered at 1150 °C is higher than for the corresponding samples sintered at 1500 °C, including differences in bulk conductivity; this agrees with results reported elsewhere [5]. The latter authors attempted to interpret this behaviour by assuming that cobalt dissolves in the lattice when the sintering temperature increases, and might increase the interaction between oxygen vacancies and the dopant.

The grain boundary conductivity also increases with a decrease in sintering temperature. This is somewhat surprising, because the average grain size increases with sintering temperature, and typical models for the effects of grain size (e.g. the brick layer model [17, 18]) predict a decrease in grain boundary resistance. However, Lewis et al. [6] identified isolated regions of cobalt containing

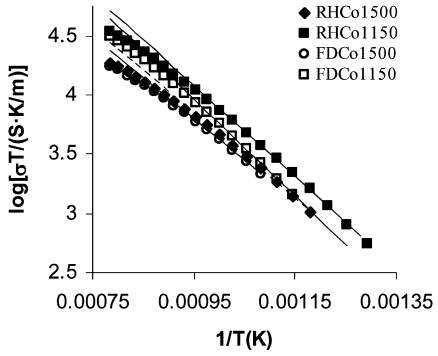

Fig. 5 Total conductivity results for the samples RHCo1150, RHCo1500, FDCo1150 and FDCo1500, at temperatures above 500 °C

Table 2 Values of total conductivity at 700 °C, bulk and grain boundary conductivities at 300 °C, and activation energies for the bulk and grain boundary conductivities for samples with 2% Co

Sample	σ_t (S/m) at 700 °C	σ_{bulk} (S/m)	$E_{a\text{-}bulk}$ (kJ/mol)	$L/(AR_{gb})$ (S/m)	$E_{a\text{-}gb}$ (kJ/mol)
RHCo1150	6.18	0.014	85.9	0.07	105.1
RHCo1500	3.85	0.008	91.5	0.007	103.1
FDCo1150	4.61	0.012	86.5	0.005	98.6
FDCo1500	3.48	0.010	85.7	0.004	102.3

traces of silica in a CGO + 1% Co sample sintered below 1000 °C, and argued that amorphous cobalt oxide segregated in the grain boundary may act as a cleaner of silica in the grain boundary, enhancing its conductivity. This interpretation is plausible because impurities, and mainly silica, play a negative role in the grain boundary conductivity [3].

Thus, the lower Co content in the grain boundary of samples sintered at 1500 °C might spoil the cleaning effect, rendering the grain boundaries more resistive. A confirmation of this was obtained by using the grain boundary relaxation frequency, and a typical value of the dielectric constant, as follows [15]:

$$\sigma_{gb} = 2\pi f_{gb}\varepsilon_0\varepsilon_r \tag{2}$$

This expression was derived from the expected relation between relaxation frequency, resistance and capacitance: $2\pi f_{gb}C_{gb}R_{gb} = 2\pi f_{gb}\epsilon_0\epsilon_r/\sigma_{gb} = 1$. Thus, one may estimate the values of the grain boundary conductivity even without knowing the effective geometric factor, $(L_{gb}/A) = (L/A)(\delta_{gb}/d_g)$, which is dependent on the thickness of a single boundary, δ_{gb}, and average grain size, d_g, as presented elsewhere [18]. The results shown in Fig. 6 were thus calculated on combining the experimental values of the grain boundary relaxation frequency with a typical value of the dielectric constant, $\epsilon_r \approx 30$ (see also [15]). Since the estimates of the grain boundary conductivity obtained in this way are independent of the microstructural details (e.g. grain size) and the thickness of a generic single grain, one may assume that the differences shown in Fig. 6 indicate

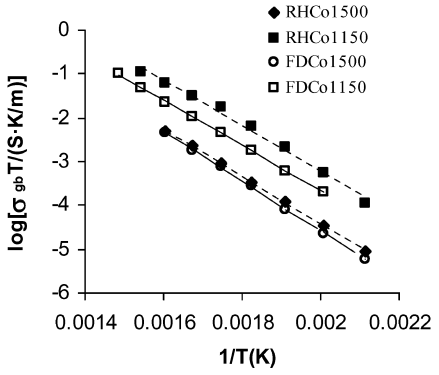

Fig. 6 Estimates of grain boundary conductivity (Eq. 2) for the samples RHCo1150, RHCo1500, FDCo1150 and FDCo1500, obtained on combining the grain boundary relaxation frequency and a typical value of the dielectric constant for ceria-based materials

significant changes in grain boundary behaviour. This can be ascribed to a decrease in Co at the grain boundaries with increasing temperature.

n-type electronic conductivity

The electronic conductivity can be calculated from the steady-state current–voltage under ion-blocking conditions [9, 10, 11]. The dependence of the n-type and p-type electronic conductivity on the oxygen partial pressure is often described by:

$$\sigma_n = \sigma_n * \left(\frac{p(O_2)}{p(O_2)*}\right)^{-1/n}; \quad \sigma_p = \sigma_p * \left(\frac{p(O_2)}{p(O_2)*}\right)^{1/n} \tag{3}$$

where n is close to 4 in generic analytical solutions and σ_n* and σ_p* are the n-type and p-type electronic conductivities at the reference electrode oxygen partial pressure, which in the present conditions is $p(O_2)^* = 0.21$ atm. For $n = 4$ one may write the total electronic current through the cell as a function of the voltage between the two electrodes as [19, 20, 21]:

$$I = \frac{nART}{4LF}\left\{\sigma_n * \left[\exp\left(\frac{4FV_0}{nRT}\right) - 1\right] + \sigma_p * \left[1 - \exp\left(-\frac{4FV_0}{nRT}\right)\right]\right\} \tag{4}$$

where V_0 is the voltage between the reference and ion-blocking electrodes; L is the thickness of the sample, A is the surface area of the platinum electrodes, and R, T and F have their usual meanings. Actually, the exponent of the power law dependence of the n-type and p-type conductivities on the oxygen partial pressure may deviate from $-1/4$ and/or $1/4$, and one should rather differentiate I versus V_0 to obtain the electronic conductivity [5, 11]:

$$\sigma_e = \frac{L}{A}\frac{dI}{dV_0} \tag{5}$$

The Nernst equation relates the values of $p(O_2)$ and V_0:

$$p(O_2) = p(O_2)^{ref} \exp\left(-\frac{4FV_0}{RT}\right) \quad (6)$$

Figure 7 shows the ion-blocking results obtained for the samples RHCo1150 and RHCo1500, prepared from commercial nanopowder, and Fig. 8 shows the corresponding dependence of n-type conductivity on the oxygen partial pressure. Sintering at lower temperature thus displaces the onset of the n-type conductivity to slightly more reducing conditions. The slope in this representation varies from about $-1/5$ to $-1/6$, thus showing that the exponent of the power law dependence of the electronic conductivity on oxygen partial pressure deviates from $-1/4$. This invalidates Eq. 4, and indicates that numerical differentiation of I versus V_0 is a more correct method to obtain the electronic contribution, as proposed elsewhere [5, 11], without imposing assumptions about the dependence of n- or p-type electronic conductivity on the oxygen partial pressure.

Figure 9 shows the temperature dependence of n-type conductivity for a typical value of the oxygen partial pressure, $p(O_2) = 10^{-12}$ atm. A summary of the results for these and other samples is shown in Table 3. These

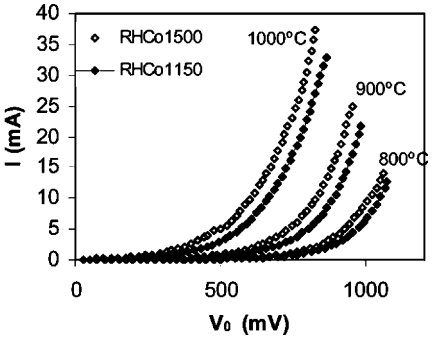

Fig. 7 Ion-blocking results obtained for the samples RHCo1150 and RHCo1500

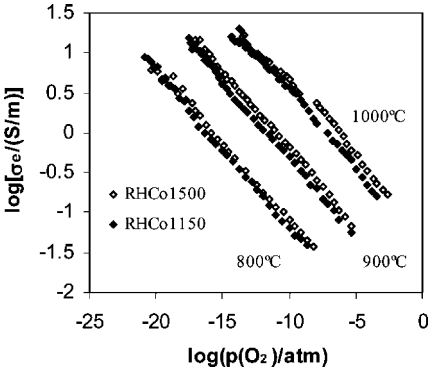

Fig. 8 n-type conductivity of the samples RHCo1150 and RHCo1500, extracted from ion-blocking experiments by numerical differentiation (Eq. 5) and using the Nernst equation to obtain the values of $p(O_2)$

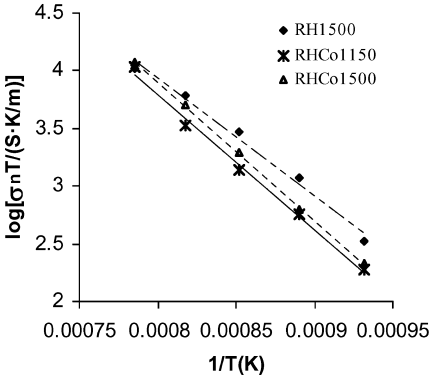

Fig. 9 Temperature dependence of the n-type conductivity of the samples RH1500, RHCo1500 and RHCo1150, at $p(O_2) = 10^{-12}$ atm

Table 3 n-type electronic conductivity and activation energy at $p(O_2) = 10^{-12}$ atm between 800–1000 °C for samples prepared from commercial and freeze-dried precursors

Sample	T (°C)	σ_e (S/m)	E_a (eV)
RHCo1150	1000	8.42	2.32
	900	1.17	
	800	0.17	
RHCo1500	1000	9.20	2.38
	900	1.65	
	800	0.20	
RH1500	1000	8.23	2.02
	900	2.49	
	800	0.31	
FDCo1150	1000	13.43	2.34
	900	1.76	
	800	0.27	
FD1600	1000	–	2.42
	900	2.55	
	800	0.28	

results clearly confirm that additions of Co suppress the n-type conductivity. This effect is less pronounced in samples fired at higher temperature, probably because Co is partially lost by volatilization and/or is redistributed differently in the microstructures of samples fired at 1150 °C and 1500 °C.

Similar conclusions can be drawn from the results obtained for samples prepared from a different FD precursor (Fig. 10 and Table 3). However, significant differences are found for the samples FDCo1150 and RHCo1150, prepared from different precursor powders, probably due to significant microstructural differences between these samples. Note also that the average grain size of the FD precursor (about 100 nm) is somewhat larger than for the corresponding commercial RH powder (about 20 nm).

Conclusions

Samples of 2% Co-CGO showed that relative density, total conductivity and bulk and grain boundary con-

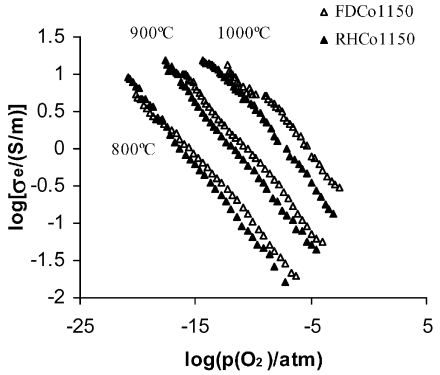

Fig. 10 Comparison of n-type conductivity results obtained for the samples RHCo1150, obtained from commercial nanopowders, and FDCo1150, obtained from a freeze-dried precursor

ductivities increase when the sintering temperature decreases from 1500 °C to 1150 °C. The grain boundary behaviour is clearly changed by additions of Co, probably because Co acts as a cleaning agent against impurities which are responsible for the blocking effect of grain boundaries. Additions of Co may thus play several beneficial effects, including the ability to attain high density at lower temperatures, improved mechanical resistance due to finer grain sizes, and less resistive grain boundaries. These effects are spoiled when excessive temperatures are used.

Additions of Co also affect the onset of n-type conductivity, which is displaced to more reducing conditions, thus extending the electrolytic domain slightly. The greatest effect is attained in samples with Co additions and fired at relatively low temperatures. Co additions become less effective on the n-type conductivity when the sintering temperature was increased. It seems that Co-rich grain boundaries might play opposite effects on the onset of n-type conductivity under reducing conditions, and on the ionic conductivity which predominates under oxidizing conditions.

Acknowledgements The authors acknowledge the financial support by the Spanish Research Program MCyT (MAT-2001-3334); by the Canary Islands Government (PI/2001/053); by FCT, Portugal, under contract POCTI/CTM/39381/2001; and by "Accion Integrada" HP01-82. We also thank M.E.C.D. for a F.P.U. grant (D.P.C) and "Convenio Cajacanarias-ULL" for another grant (D.M.L.).

References

1. Inaba H, Tagawa H (1996) Solid State Ionics 83:1
2. Yamamoto O (2000) Electrochim Acta 45:2423
3. Steele BCH (2000) Solid State Ionics 129:95
4. Kleinlogel C, Gauckler LJ (2000) Solid State Ionics 135:567
5. Fagg DP, Abrantes JCC, Pérez-Coll D, Núñez P, Kharton VV, Frade JR (2003) Electrochim Acta 48:1023
6. Lewis GS, Atkinson A, Steele BCH (2000) In: Bossel U (ed) Proceedings of the 4th Europe SOFC forum, vol 2. Oberrohrdorf, Switzerland, p 773
7. Zhang T, Hing P, Huang H, Kilner J (2002) J Eur Ceram Soc 22:27
8. Wang S, Kobayashi T, Dokiya M, Hashimoto T (2000) J Electrochem Soc 147:3606
9. Hebb M (1952) J Chem Phys 20:185
10. Navarro L, Marques F, Frade JR (1997) J Electrochem Soc 144:267
11. Lübke S, Wiemhöfer H-D (1999) Solid State Ionics 117:229
12. Riess I, Braunshtein D, Tannhauser DS (1981) J Am Ceram Soc 64:480
13. Adham KE, Hammou A (1983) Solid State Ionics 9–10:905
14. Christie GM, van Berkel FPF (1996) Solid Sate Ionics 83:17
15. Pérez-Coll D, Núñez P, Frade JR, Abrantes JCC (2003) Electrochim Acta 48:1551
16. Huang K, Feng M, Goodenough JB (1998) J Am Ceram Soc 81:357
17. Santos AP, Domingues RZ, Kleitz M (1998) J Eur Ceram Soc 18:1571
18. Abrantes JCC, Labrincha JA, Frade JR (2000) J Eur Ceram Soc 20:1603
19. Marques RMC, Marques FMB, Frade JR (1994) Solid State Ionics 73:15
20. Marques RMC, Marques FMB, Frade JR (1994) Solid State Ionics 73:27
21. Kim JH, Yoo HI (2001) Solid State Ionics 140:105